

# Analysis of a High- $T_c$ Hot-Electron Superconducting Mixer for Terahertz Applications

H. S. Karasik<sup>\*)</sup>, W.R. McGrath, and A.L. C. Gaidis

*Center for Space Microelectronics Technology, Jet Propulsion Laboratory,  
California Institute of Technology, Pasadena, CA 91109*

The prospects of a  $\text{YBa}_2\text{Cu}_3\text{O}_{7-\delta}$  (YBCO) hot-electron bolometer (HEB) mixer for a THz heterodyne receiver is discussed. The modeled device is a submicron bridge made from a 10 nm thick film on a high thermal conductance substrate. The mixer performance expected for this device is analyzed in the framework of a two-temperature model which includes heating both of the electrons and the lattice. Also, the contribution of heat diffusion from the film through the substrate and from the film to the normal metal contacts is evaluated. The intrinsic conversion efficiency and the noise temperature have been calculated as functions of the device size, local oscillator (L.O) power, and ambient temperature. Assuming thermal fluctuations and Johnson noise to be the main sources of noise, a minimum single sideband (SSB) mixer noise temperature of  $\approx 2000$  K is predicted. For our modeled device, the intrinsic conversion efficiency at an IF of 2.5 GHz is 10 dB or better and the required local oscillator power is  $\sim 10$   $\mu\text{W}$ .

PACS:

85.25.Am Superconducting device characterization, design and modeling

84.25.Pb Superconducting infrared, submillimeter and millimeter wave detectors

07.57.Kp Nonlinear; infrared, submillimeter wave, microwave, and radiowave receivers and detectors

07.87.+v Spaceborne and space research instruments, apparatus, components (satellites, space vehicles, etc.)

<sup>\*)</sup> E-mail: karasik@kbs-mac.jpl.nasa.gov

## 1. introduction

The superconductive hot-electron bolometer (HEB) [1,2] is presently considered the most promising heterodyne mixer device for the terahertz (THz) frequency range. Recent experiments with a Nb HEB mixer demonstrated a 560 K double-sideband (DSB) noise temperature at 533 GHz, and should remain relatively low for radiation frequencies up to at least 10 THz [3]. Currently, the most competitive mixer available at THz frequencies is a Schottky-diode mixer with a typical SSB noise temperature at 2.5 THz, for example of 20,000 K and I.O power  $\sim 1$ -3 mW. The HEB mixer can be especially useful in space-borne applications for atmospheric research if operated at elevated temperatures where low-power mechanical cryocoolers are readily available and where requirements for a low I.O power are critical. For such an application, a HEB device made from a thin YBCO film can be used. The fabrication technology for such films has been significantly improved since the discovery of high- $T_c$  superconductivity. Now, ultrathin films having a thickness  $d$  down to a few unit cells have been successfully fabricated [4- 9]. The critical temperature  $T_c > 85$  K and superconducting transition width  $\delta T_c = 1$ -2 K are typical for films with  $d \geq 10$  nm, and a critical current density  $j_c = 8 \times 10^6$  A/cm<sup>2</sup> was observed in 10 nm thick films at 77 K [8]. Fabrication of superconducting structures made from YBCO with in-plane sizes 100-500 nm has also been demonstrated [10- 13]. Critical current densities as large as  $5 \times 10^6$  A/cm<sup>2</sup> have been measured in 200 nm wide superconducting lines [14]. A variety of materials (e.g. MgO, LaAlO<sub>3</sub>, NdGaO<sub>3</sub>, YSZ) have been found to provide a moderate dielectric constant and epitaxial YBCO film growth. Also, the use of buffer layers allows growth of YBCO films on silicon and sapphire (YSZ buffer layer for Si and CeO<sub>2</sub> for sapphire). With such promising film growth technology, it becomes important to now examine the theoretical issues involved in designing optimum devices.

In contrast to slow bulk bolometric detectors, an HEB mixer can operate with a high intermediate frequency (IF) of the order of several gigahertz, and under appropriate I.O power. This sets quite different from detector device criteria for mixer device optimization. In this paper we give a detailed analysis of the thermal processes important for optimum HEB mixer performance. Within the framework of a model which includes the temperature of both the

electrons and photons, expressions for mixer conversion efficiency, and II impedance have been derived, which are valid for a wide range of  $H_c$ . The contributions of both electron temperature fluctuations and Johnson noise in the mixer noise temperature have been investigated as functions of  $d_c$  and  $J_c$  power. The requirements for the substrate thermal conductivity in relationship to the device in-plane size have been determined. Specific examples are given for  $H_c \approx 2.5$  GHz, which is a practical frequency for remote sensing applications in astrophysics and atmospheric science. A SSB noise temperature  $\approx 2000$  K is predicted for an optimized device and mixer circuit.

## II. Nonequilibrium Photoreponse and Thermal Relaxation in $d_c$ YBC Film/Substrate System.

A wide band of intermediate frequencies is possible in high- $T_c$  YBCO films due to the fast nonequilibrium photoreponse inherent in the material. The origin of the response has been studied for a number of years. Recent frequency-domain [15,16] and time-domain [17] measurements demonstrate that the resistive response to radiation can be adequately described in terms of a relaxation of the electron temperature  $T_e$  via interaction with phonons with a characteristic time  $\tau_{ep}$  of 1-2 ps at 80-90 K, and of a slower relaxation of the phonon temperature  $T_p$ . The time constant of the latter quantity depends on the film size and substrate material. One should point out that the mixer response time in a lumped low- $T_c$  HJB is determined by  $\tau_{ep}$  only, since the escape time for phonons in  $\sim 10$  nm thick films is much shorter, that is, the phonons remain in equilibrium with a heat sink.

The principal heat removal processes for a high- $T_c$  bolometer are shown in a flow diagram in Fig. 1. The bolometer is modeled as a thin film microbridge with normal contacts. The nonequilibrium electrons in the microbridge heated by the absorbed rf radiation and dc transport current give their energy to phonons during a very short electron-phonon energy relaxation time  $\tau_{ep}$ . The electron diffusion mechanism of heat transport which is especially important in submicron Nb HJB mixers [2,3] is less significant in submicron YBCO device due to the very short electron diffusion length. The characteristic electron diffusion length can be estimated as  $l_d \approx \pi \sqrt{D_e \tau_{ep}}$

The electron diffusivity  $D_e$  can be found as  $D_e = \kappa_e / c_e$ , where  $\kappa_e$  is the electron thermal conductivity [18], and  $c_e$  is the electron specific heat per unit volume [19]. The data of Table 1 give  $D_e \approx 2.5 \text{ cm}^2/\text{s}$ , thus  $l_d \approx 60 \text{ nm}$ , suggesting that electron diffusion may speed up the electron thermal energy relaxation by  $\approx 30\%$  in ultra-short devices with a length  $L \approx 0.1 \text{ }\mu\text{m}$ .

The nonequilibrium phonons leave the film either through the film-substrate boundary or by diffusing to the normal metal contacts. The phonon escape to the substrate is generally dominated by an acoustic mismatch, or thermal boundary resistance  $R_b = \tau_{es} / (c_p d)$ , where  $\tau_{es}$  is the phonon escape time and  $c_p$  is the phonon specific heat per unit volume [20]. The value of  $R_b$  is fairly constant in the temperature range 70–100 K and has been measured for various substrates. One of the lowest reported values of  $R_b$  is  $5 \times 10^{-4} \text{ cm}^2 \text{K/W}$  for MgO substrates [21,22], giving  $\tau_{es} \approx 33d \text{ ps}$  for  $d$  in nm. Such values of  $\tau_{es}$  have been directly measured in a number of experiments [15,16,22–24]. The diffusion time of phonons to the contacts can be estimated as  $\tau_{diff} \approx L^2 / (\pi^2 D_p)$ , where  $D_p$  is the phonon diffusivity. Determining  $D_p = \kappa_p / c_p$  ( $\kappa_p$  is the phonon thermal conductivity [25], see Table 1.), we obtain  $D_p \approx 0.15 \text{ cm}^2/\text{s}$ . One can see that  $\tau_{diff} \approx \tau_{es}$  when  $L \approx 0.1 \text{ }\mu\text{m}$  and  $d \approx 10 \text{ nm}$ . Thus, for submicron bridge lengths the cooling due to the phonon diffusion should play a role. For longer samples the diffusion time increases rapidly. In general, the effective time of phonon escape is  $\tau_{eff} \approx \tau_{es} + \tau_{diff}^{-1}$ .

Yet another thermal process affecting the microbridge thermal relaxation speed and the total thermal resistance is the diffusion of heat in the substrate. If the characteristic in-plane device size  $L$  is chosen to be much smaller than the substrate thickness  $d_s$ , the effective thermal resistance of the substrate is found as [26]:

$$R_s = \left\{ \frac{S \kappa_s}{a} \sqrt{\left[ 1 + \frac{a}{l_s(f)} \right]^2 + \left[ \frac{a}{l_s(f)} \right]^2} \right\}^{-1}, \quad (1)$$

where  $\kappa_s$  is the thermal conductivity of the substrate,  $a$  is the equivalent radius of the device area through which heat flows into the substrate,  $l_s = \sqrt{D_s/(2\pi)}$  is the effective length of diffusion at modulation frequency  $f$ ,  $D_s$  is the phonon diffusivity of the substrate, and  $S$  is the device area. For a device with a square shape of side  $L$ ,  $a = L/\sqrt{\pi}$ . Although the total thermal resistance,  $R_{T_s}$ , decreases, the thermal resistance per unit area,  $R_{T_s}L^2$ , becomes larger if the device has larger area

The optimization of the total thermal resistance between an electron subsystem and a heat sink as well as its modulation frequency dependence is quite important for the HEB mixer operation. A rule of thumb is that the thermal resistance should be made as low as possible and its frequency dependence should be as flat as possible. The minimum thermal resistance determines the maximum LO power contributing to the IF signal. A pronounced frequency dependence of the thermal resistance generally yields a loss of power at the IF of interest with respect to the maximum attainable conversion efficiency at a zero IF. The contributions from thermal boundary resistance and from the substrate is compared in the following section.

### III. Conversion Efficiency      IF Impedance      in a Two-Temperature Model.

In contrast to a low- $T_c$  HEB mixer, a high- $T_c$  HEB mixer cannot be described in terms of the electron temperature only. This is because at temperatures  $\sim 90$  K the phonon heat capacity is always much larger than that of the electrons. A more appropriate approach [27] makes use of a "two-temperature" model describing the dynamics of the electron and phonon temperatures which are both different from the temperature of the heat sink. This is the approach we use here.

The coupled differential equations for the electron and phonon temperatures are given in [28]. The following spectrum of the electron temperature was obtained:

$$\Delta T_e = \alpha P_{rf} \frac{\tau_{ep} + (c_e/c_p)\tau_{es}}{c_e V} \left[ \frac{1 + (\omega\tau_\phi)^2}{\sqrt{[1 + (\omega\tau_1)^2][1 + (\omega\tau_2)^2]}} \right], \quad (2)$$

where  $\alpha$  is the rf coupling factor,  $P_{rf}$  is the amplitude of the incident rf power,  $V$  is the bolometer volume,  $\tau_\phi$ ,  $\tau_1$ , and  $\tau_2$  are given by the following formulas:

$$\tau_{1,2}^{-1} = \tau_{\pm s}^{-1} - \frac{1}{2\tau} \left[ \mp \sqrt{1 - 4 - \frac{\tau^2}{\tau_{ep}\tau_{es}}} \right],$$

$$\tau^{-1} = \tau_{es}^{-1} + \tau_{ep}^{-1} + \tau_p^{-1}$$

$$\tau_\phi^{-1} = \tau_{es}^{-1} + \tau_p^{-1}$$

$$\tau_p = \tau_{ep} c_p / c_e \quad (3)$$

In YBCO  $\tau_{ep}$  is so short that  $\tau_p \ll \tau_{es}$ . This condition, along with  $c_p \gg c_e$ , allows one to simplify Eqn's. 3:

$$\tau_1 \approx \tau_{ep}, \quad \tau_2 \approx \tau_{es}, \quad \tau_\phi \approx \tau_p \quad (4)$$

and obtain the following spectrum of the electron temperature:

$$\Delta T_e \approx \alpha P_{rf} \frac{\tau_{ep} + (c_e/c_p)\tau_{es}}{c_e V} \left[ \frac{1 + (\omega\tau_p)^2}{\sqrt{[1 + (\omega\tau_{ep})^2][1 + (\omega\tau_{es})^2]}} \right] \quad (5)$$

This frequency dependence for a response in thin YBCO films was observed in recent optical mixing experiments at  $\lambda = 1.54 \mu\text{m}$  [27] and  $\lambda = 9.6 \mu\text{m}$  [29] (see Fig. 2).

From Fig. 5 one can obtain the effective thermal resistance between electrons and substrate:

$$R_{e-s} = \frac{\Delta T_c}{\alpha I_{rad}} \left[ \tau_{qp} / (\epsilon_s V) \quad R_b / S \right] \sqrt{\frac{1 + (\omega \tau_p)^2}{1 + (\omega \tau_{qp})^2} [1 + (\omega \tau_{cs})^2]} \quad (6)$$

and the total thermal resistance to the bath is

$$R_{tot} = R_{e-s} + R_s \quad (7)$$

Figure 3(a-d) shows the behavior of  $R_s$ ,  $R_{e-s}$  and  $R_{tot}$  for two widely used substrates (MgO and LaAlO<sub>3</sub>) and two device sizes ( $L = 10 \mu\text{m}$  and  $L = 1 \mu\text{m}$ ). The YBCO film thickness is 10 nm in all cases.  $R_s$  dominates for poor thermal conducting substrate, large device sizes, and low Hf: (see LaAlO<sub>3</sub> for  $L = 10 \mu\text{m}$  in Fig. 3a). We should point out that Fig. 7 underestimates the total thermal resistance since the reverse flow of phonons from the substrate to the YBCO film is not taken into account. The effect should be larger for larger device areas and lower substrate thermal conductivity. Nevertheless, it is believed that MgO substrates, where  $R_s \ll R_{e-s}$ , are nearly ideal. In addition,  $R_s$  becomes negligible for submicron-size devices (which are needed to minimize I/O power requirements) and will not be considered in the following analysis.

Equations 2 and 5 were obtained assuming no self-heating effects in the superconducting film (small dc current) and a simple, linear (with respect to the electron temperature shift) dependence for the heat flow from electrons to phonons. The latter assumption is applicable for only small differences between  $T_c$  and  $T_p$ . It has been found experimentally that in YBCO films,  $\tau_{qp} \sim T_c^{-1}$  [30], hence the heat flow from electrons to phonons is actually proportional to  $T_c^{-3} \cdot T_p^{-3}$ .

Here we discuss the more realistic situation where the device is so far from equilibrium that one can neglect neither the non-linearity in the heat conductance (strong pumping), nor the self-heating caused by transport current. We also include in the model the feedback effect from the Hf load impedance influencing the mixer conversion efficiency and modifying the mixer bandwidth [31]. The phonon diffusion to the contacts is taken into account

approximately by assuming the bolometer is lumped element with an appropriate "diffusion channel" heat conductance between the center of the microbridge and the contacts incorporating a diffusion channel.

We start with the following dynamic heat-flow equations:

$$c_e V_d \frac{dT_e}{dt} = -AV_d(T_e^3 - T_p^3) + IV_b + \alpha P \quad (8a)$$

$$c_p V_d \frac{dT_p}{dt} = AV_d(T_e^3 - T_p^3) - \frac{S}{R_b}(T_p - T) - \frac{8\kappa_p}{L^2} V_d(T_p - T). \quad (8b)$$

Here  $V_d$  is the volume of the microbridge,  $A = \gamma/(3\tau_{ep}T)$  ( $\gamma$  is the Sommerfeld constant) is the constant characterizing the coupling strength of the electrons to the phonons, and  $V_b$  and  $I$  are the bias voltage and current, respectively. The last term in Eq. 8b represents a one-dimensional heat flow due to the phonon diffusion to the contacts. It assumes that  $T_p$  is the phonon temperature in the center of the bridge, and  $\kappa_p$  is temperature independent. Since we are interested in a periodic solution, the following substitutions can be made  $P = P_0 + \tilde{P}e^{j\omega t}$ ,  $T_e = T_{e0} + \tilde{T}_e e^{j\omega t}$ ,  $T_p = T_{p0} + \tilde{T}_p e^{j\omega t}$ ,  $V_b = V_{b0} + \tilde{V}_b e^{j\omega t}$ ,  $I = I_0 + \tilde{I} e^{j\omega t}$ ,  $R = R_0 + \tilde{R} e^{j\omega t}$ , where  $\tilde{P}$ ,  $\tilde{T}_e$ ,  $\tilde{T}_p$ ,  $\tilde{V}_b$ ,  $\tilde{I}$ , and  $\tilde{R}$  are the complex amplitudes of the corresponding quantities. Eqn's. 8 are now split into two systems for the dc values

$$AV_d(T_{e0}^3 - T_{p0}^3) - I_0 V_{b0} + \alpha P_0 = 0 \quad (9a)$$

$$AV_d(T_{e0}^3 - T_{p0}^3) - \frac{S}{R_b}(T_{p0} - T) - \frac{8\kappa_p}{L^2} V_d(T_{p0} - T) = 0, \quad (9b)$$

and for the 1st harmonics

$$(j\omega c_e + 3AT_{e0}^2)V_d \tilde{T}_e = 3AV_d T_{p0}^2 \tilde{T}_p + I_0 \tilde{V}_b - V_{b0} \tilde{I} + \alpha \tilde{P} \quad (10a)$$

$$(j\omega c_p + c_p/\tau_{es} + 8c_p D_p/L^2 + 3AT_{p0}^3)\tilde{T}_p = 3AT_{e0}^3\tilde{T}_e \quad (10b)$$

Expression 10b implies that the effective time constant due to the phonon diffusion is  $\tau_{diff} = L^2/(8D_p)$ .

The expression for the HEB voltage responsivity can be obtained as:

$$S_V \equiv \tilde{V}_b/\tilde{P} = \frac{\alpha C}{I_0} \frac{R_L}{R_L + R_0} \frac{1 + j\omega\tau_0}{\left[ \tau_0/\tau_{es}^* - \omega^2\tau_{ep}\tau_0 + j\omega(\tau_{ep} + \tau_0) \right] + C \frac{R_0 - R_L}{R_0 + R_L} (1 + j\omega\tau_0)}, \quad (11)$$

where  $R_L = \tilde{V}_b/\tilde{I}$  is the IF load resistance, and  $R_0 = V_{b0}/I_0$  is the dc resistance of the device,

$\tau_0 = \tau_p/\left[ \tau_p/\tau_{es}^* + (T_{p0}/T_{e0})^{n-1} \right]$ ,  $\tau_{es}^* = (\tau_{es}^{-1} + \tau_{diff}^{-1})^{-1}$ . The next step is to relate the single sideband (SSB) mixer conversion efficiency to the voltage responsivity. As is well-known [1,2], an ac voltage across the mixer IF load,  $R_L$ , is given by  $V_{if} = 2\tilde{S}_V\sqrt{P_s P_{L,O}} \exp[j(\omega t + \phi)]$ , where  $P_s$  is the signal power. Then the conversion efficiency is given by:

$$\eta = \frac{|P_{if}|}{P_s} = \frac{2|\tilde{S}_V|^2 P_{L,O}}{R_L P_{DC}} = \frac{2\alpha^2 C^2 P_{L,O}}{(R_0 + R_L)^2} \left| \frac{1 + j\omega\tau_0}{\left[ \tau_0/\tau_{es}^* - \omega^2\tau_{ep}\tau_0 + j\omega(\tau_{ep} + \tau_0) \right] + C \frac{R_0 - R_L}{R_0 + R_L} (1 + j\omega\tau_0)} \right|^2. \quad (12)$$

One can verify that in the low temperature limit, when  $\tau_{es} \ll \tau_p \ll \tau_{ep}$ , the frequency dependent term in the product given by Eq. 12 reduces to  $|1 + j\omega\tau_{ep}/[1 + C(R_0 - R_L)/(R_0 + R_L)]|^{-2}$ , giving the expression previously obtained in [31,32].

The IF impedance can be expressed as  $Z(\omega) = R_0 + (\partial R/\partial T_e)\tilde{T}_e$  (see Ref. 32 for a detailed derivation). Then using Eqn's. 8, one can obtain

$$Z(\omega) = R_0 \frac{\left[ \tau_0 / \tau_{es}^* - \omega^2 \tau_{ep} \tau_0 + j\omega(\tau_{ep} + \tau_0) \right] + C(1 + j\omega\tau_0)}{\left[ \tau_0 / \tau_{es}^* - \omega^2 \tau_{ep} \tau_0 + j\omega(\tau_{ep} + \tau_0) \right] - C(1 + j\omega\tau_0)} \quad (13)$$

which coincides in the low-temperature limit with the following expression from [32]:

$$Z(\omega) = R_0 \frac{1 + C \frac{1 + j\omega \tau_{es}}{1 + \Gamma}}{1 - C \frac{1 + j\omega \tau_{ep}}{1 - \Gamma}} \quad (14)$$

#### IV. Noise Temperature.

The expression for the noise temperature due to the electron temperature fluctuations of a low- $T_c$  HEB mixer was given in [32]. It was also shown that this quantity does not depend on the conversion efficiency, and thus may be fairly universal. We believe it is applicable for a high- $T_c$  HEB mixer, and the corresponding SSB noise temperature contribution is given by:

$$T_M^{TF} = \frac{2T_{e0}^2 G_e}{\alpha^2 P_{LO}} \quad (15)$$

where  $G_e = 3AV_d T_e^{-2}$  is the thermal conductance between electrons and phonons.

The contribution of Johnson noise should be evaluated by taking into account the enhancement of the noise due to the self-heating in a bolometer. Simply, one can use the equivalent noise circuit introduced in [33] (see Fig. 4). Following [32,33], we assume that the classical Johnson noise source  $e_j = \sqrt{4k_B R_0 T_{e0}}$  must appear twice in the bolometer equivalent circuit. Source  $e_j$  acts simply as a voltage source in series with the bolometer

impedance  $Z(\omega)$ . The source  $E/2 = -e_f/2$  is placed to take into account the output noise enhancement caused by the self-detection of the Johnson noise in the bolometer. The impedance  $Z_x$  represents the bolometer reactance due to its thermal inertia and self-heating contribution.  $Z_x$  is chosen to agree with Eq. 14 for the bolometer HF impedance, that is,  $Z_x = ZR/(Z + R)$ . Due to the frequency dependence of impedance  $Z_x$ , a "white" noise  $e_f$  becomes frequency dependent at the load  $R_L$ . The corresponding expression for the noise temperature is obtained by dividing the noise power dissipated in the load by the conversion efficiency given in Eq. 13. A relatively simple expression for Johnson noise has been obtained for a low- $T_c$  HEB mixer [32]. However, for the high- $T_c$  case the expression turns out to be very cumbersome, therefore we just calculate the noise temperature numerically.

## V. Numerical Results.

Numerical simulations were performed for an HEB mixer with parameters which represent realistic estimates for a device to be used in practical cryocooled mixer applications: an area of  $0.1 \times 0.1 \mu\text{m}^2$ , a thickness of 10 nm,  $T_c = 85$  K,  $\delta T_c = 2$  K, normal resistance  $R_n = 200 \Omega$ , and an operating temperature of  $T = 66$  K. A coupling factor  $\alpha$  was chosen to be 1 for simplicity ( $\alpha$  will depend on the details of the mixer embedded circuit and optics), so  $P_{LO}$  represents the 1.0 power absorbed in the device. Contour plot in Fig. 5(a) represents the results of simulations of the HEB mixer SSB noise temperature,  $T_M$  at  $f_H = 2.5$  GHz (an HF high enough for practical applications [Waters]). Figure 5(b) shows the SSB mixer conversion efficiency under the same conditions. The contours in Figs. 5(a) are plotted versus dc and 1.0 power since these are two important and experimentally variable parameters for a HEB mixer. With the given dc and 1.0 power scales, the top right corner of all plots corresponds to the normal state, the bottom left corner corresponds to a nearly superconducting state. At both of these edges the noise temperature is very high. In the nearly superconducting state, where the 1.0 power is low,  $T_M^{TF}$  is high. In the normal state, where the conversion loss is very high,  $T_M^J$  is high. Just at the middle of the resistive transition, the noise temperature reaches its minimum value ( $\sim 2000$  K) and the conversion efficiency is greater than unity. Figure 6

shows the IF spectra of the conversion efficiency and the IF impedance. The low-frequency and high-frequency plateaus in the conversion efficiency spectrum correspond, respectively, to bolometric (electrons + phonons) and hot-electron (electrons only) effects (see Fig. 2 for comparison). As seen in Fig. 6, the conversion efficiency drops by  $\approx 5$  dB over a range of IF from 1 GHz to 10 GHz. This is the result of the long time constant,  $\tau_{es}$ , due to the escape of phonons from the film to the substrate. This frequency dependence of  $\eta$  will produce a non-flat IF baseline in a practical spectroscopic receiver. However, over a range of a few GHz (wide enough for spectroscopic applications), this baseline shift is small enough to be readily compensated by backend spectrometer electronics. The optimally pumped IV characteristic is shown in Fig. 7. Both slightly underpumped and overpumped curves are presented in the same Figure. The parameters of the optimal operating point are given in Table 2.

Figure 8 shows the behavior of the noise temperature as a function of  $P_{LO}$ . The results suggest that the noise temperature minimum is formed due to an intersection of a weak descending  $T_M^{TF}(P_{LO})$  and a steep ascending  $T_M^J(P_{LO})$  dependencies in the vicinity of the middle of superconducting transition. At the LO power levels just below the optimal point the contribution of Johnson noise is very small and the thermal fluctuation noise,  $T_M^{TF}$  at  $T_c$ , represents the total mixer noise temperature. Also,  $P_{LO} \gg P_{DC}$  at the optimum operating point (see Fig. 5a and Table 2). This allows us to simplify the numerical procedure using Eq. 15 for the total minimum noise temperature estimate.  $P_{LO}$  can be found from Eqn's 9, as following:

$$P_{LO} = \left( I^2/R_b + 8\kappa_p d \right) \left( \sqrt[3]{T_c^3 - P_{LO}/(AI^2d)} - T \right), \tag{16}$$

and  $T_M$  is just given by Eq. 15.

An important practical consideration in fabricating a high- $T_c$  1 HJ mixer is device size. To analyze the effect of the device size on  $T_M$  and  $P_{LO}$  one should turn to Eqn's 9. In a linear approximation Eq. 9b can be written as

$$R_{e-ph} + R_{diff} = 1/R_b + 1/R_{diff} = 0, \tag{17}$$

where  $R_{e-ph} = (3AdT_{c0})^{-1}$  is the apparent thermal boundary resistance due to electron-phonon scattering,  $R_{diff} = I^2/(8\kappa_p d)$  is the apparent thermal boundary resistance due to phonon diffusion to the contacts.

Figure 9 shows how the different mechanisms of heat conductance relate to each other. The horizontal dashed line is a solution of  $R_{e-ph} = R_b$ , i.e.  $d_0 = (3AT_c^2 R_b)^{-1} = 1.2$  nm. The vertical dashed line is a solution of  $R_{e-ph} = R_{th}$ ,  $l_0 = \sqrt{8kp} / (3AT_c^2) = 0.07$   $\mu\text{m}$ . Whenever  $d < d_0$  and  $l < l_0$  (region I) the electron-phonon thermal resistance is a "bottle-neck" for the heat flow from the bolometer to the bath. This is the case for a low temperature IIB, i.e. the phonons remain in equilibrium with the heat sink ( $T_{p0} = T$ ). It gives

$$P_L = AT_c^2 d (T_c^3 - T^3) \quad \text{and} \quad T_M = 6T_c^4 / (T_c^3 - T^3) \quad (18)$$

This noise temperature is the lowest and  $P_{LO}$  is the highest under given conditions. However, both  $d_0$  and  $l_0$  are so small that this case has rather limited practical value.

In region II of a diagram in Fig. 9 the phonon escape to the substrate dominates over the phonon in-plane diffusion. Therefore,  $l^2(T_{p0} - T) / R_b = l^2 A d (T_c^3 - T_{p0}^3) = P_{LO}$  (see Eq. 9b). In the limit of a thick film  $T_{p0}$  approaches  $T_{p0} (\approx T_c)$  (conventional bolometer), i.e.

$$P_{LO} = l^2 (T_c - T) / R_b \quad \text{and} \quad T_M = \frac{3AR_b T_c^4}{T_c - T}. \quad (19)$$

In region III the diffusion to the contacts dominates, i.e.  $8\kappa_p d (T_{p0} - T) A l^2 d (T_c^3 - T_{p0}^3) = P_{LO}$ . For a large area device  $T_{p0} \approx T_c$  and

$$P_{LO} = 8\kappa_p d (T_c - T) \quad \text{and} \quad T_M = \frac{3AT_c^4 l^2}{4\kappa_p (T_c - T)}. \quad (20)$$

Several examples of the size dependencies are given in Fig. 10. According to the above terminology, curves I and II belong to region II, whereas curves 4 and 4' rather belong to region III. The general trend is that a minimization of the device sizes always leads to a decrease of both noise temperature and I.O. power.

The increase of the bath temperature always leads to a degradation of the noise temperature (see Fig. 11). The I.O power, however, decreases with  $T$  and can be of a few microwatts (see also Table 2). The latter circumstance can be extremely critical at terahertz frequencies where compact powerful local oscillators are not readily available. A necessary trade-off between a sufficiently low noise temperature and available I.O power should be found for each practical case.

## **VI. Conclusion.**

We have developed a comprehensive model of the thermal processes in a high- $T_c$  HEB mixer. It was shown that the heat conductance from electron to phonons, escape of phonons through the film/substrate interface, and the phonon diffusion to the contacts are the most critical processes in determining the device response and sensitivity. Using a two-temperature model, all important mixer parameters were calculated and studied for a range of conditions needed for a practical THz heterodyne receiver. The effects of device size and of heat sink temperature have been evaluated. It was demonstrated that a submicron-size device made of a 10 nm thick film can have a very low noise temperature (a few thousand Kelvin) and require only microwatts of I.O power. These combination of parameters are very favorable for space-borne heterodyne instruments operating at terahertz frequencies

The research described in this paper was performed by the Center for Space Microelectronics Technology, Jet Propulsion Laboratory, California Institute of Technology, and was sponsored by the National Aeronautics and Space Administration, Office of Mission to Planet Earth, and the Office of Space Access and Technology.

## References.

- [1] E.M. Gershenzon, G.N. Goltsman, I.G. Gogolize, Y.P. Gusev, A.I. Ilanov, B.S. Karasik, and A.D. Semenov, *Sverhprovodimost' (KIAE)* 3, 2143 (1990)[*Sov. Phys. Superconductivity* 3, 1582 (1990)]
- [2] D.H. Prober, *Appl. Phys. Lett.* **62**, 2119 (1993).
- [3] A. Skalaric, W.R. McGrath, B. Bumble, H.G. LeDuc, P.J. Burke, A.A. Verheijen, R.J. Schoelkopf, and D.H. Prober, *Appl. Phys. Lett.* **68**, 1558 (1996).
- [4] T. Wang, K.M. Beuchamp, D.J.D. Berkeley, B.R. Johnson, J.-X. Liu, J. Zhang, and A.M. Goldman, *Phys. Rev. B* **43**, 8623 (1991).
- [5] T. Terashima, K. Shimura, Y. Bando, Y. Matsuda, A. Fujiyama, and S. Koniyama, *Phys. Rev. Lett.* **67**, 1362 (1991)
- [6] J.-M. Triscone, Ø. Fischer, O. Brunner, L. Antognazza, A.D. Kent, and M.G. Karkul, *Phys. Rev. Lett.* **64**, 804 (1990).
- [7] X.X. Xi, J. Geerk, G. Linker, Q. Li, and O. Meyer, *Appl. Phys. Lett.* **54**, 2367 (1989).
- [8] J. Gao, B. Hänser, and H. Rogalla, *J. Appl. Phys.* **67**, 2512 (1990).
- [9] W.P. Shen, C. Lehané, J.P. Zheng, and H.S. Kwok, *Appl. Phys. Lett.* **64**, 3175 (1994)
- [10] J. Schneider, M. Mück, and R. Wördenweber, *Appl. Phys. Lett.* **65**, 2475 (1994).
- [11] J. Schneider, H. Kohlstedt, and R. Wördenweber, *Appl. Phys. Lett.* **63**, 2426 (1993).
- [12] A.J.M. van der Harg, E. van der Drift and P. Hadley, *IEEE Trans. Appl. Superconductivity* **5**, 1448 (1995).
- [13] M.V. Pedgash, G.J. Gerritsma, D.H.A. Blank, and H. Rogalla, *IEEE Trans. Appl. Superconductivity* **5**, 1387 (1995).
- [14] H. Assink, A.J.M. v.d. Harg, C.M. Schep, N.Y. Chen, D. v.d. Mareel, P. Hadley, E.M.J.M. v.d. Drift, and J.J. Mooij, *IEEE Trans. Appl. Superconductivity* **3**, 2983 (1993).
- [15] M. Lindgren, V. Trifonov, M. Zorin, M. Danerud, D. Winkler, B.S. Karasik, G.N. Goltsman, and E.M. Gershenzon, *Appl. Phys. Lett.* **64**, 3036 (1994).

- [16] M. Danerud, D. Winkler, M. Lindgren, M. Zorin, V. Trifonov, B.S. Karasik, G.N. Gol'tsman, and E.M. Gershenzon, *J. Appl. Phys.* **76**, 1902 (1994).
- [17] A.D. Semenov, I. S. Nebosis, Yu.P. Gousev, M.A. Heisinger, and K.F. Renk, *Phys. Rev. B* **52**, 581 (1995).
- [18] M. Ikebe, H. Fujishiro, T. Naito, M. Matsukawa, and K. Noto, *Jpn. J. Appl. Phys.* **33**, 6157 (1994).
- [19] A. Junod, In: Physical Properties of High Temperature Superconductors II, Ed. I.D.M. Ginsberg, World Scientific, 1990, p. 13.
- [20] J.M. Ferreira, B.W. Lee, Y. Dalichaouch, M.S. Torikachvili, K.N. Yang, and M.B. Maple, *Phys. Rev. B* **37**, 1580 (1988); C.A. Swenson, R.W. McCallen, and K. No, *ibid.* **40**, 8861 (1989); R. Shaviv, E.F. Westrum, Jr., R.J.C. Brown, M. Sayer, X. Yu, and R.D. Weir, *J. Chem. Phys.* **92**, 6794 (1994).
- [21] C.D. Marshall, I.M. Fishman, R.C. Dorfman, C.B. Eom, and M.D. Fayer, *Phys. Rev. B* **45**, 10009 (1992).
- [22] A.V. Sergeev, A.D. Semenov, P. Kouminov, V. Trifonov, I.G. Goghidze, B.S. Karasik, G.N. Gol'tsman, E.M. Gershenzon, *Phys. Rev. B* **49**, 9091 (1994).
- [23] G.L. Carr, M. Quijada, D.B. Tanner, C.J. Hirschmugl, G.P. Williams, S. Etemad, B. Dutta, F. DeRosa, A. Inam, T. Venkatesan, and X. Xi, *Appl. Phys. Lett.* **57**, 2725 (1990).
- [24] N. Bluzer, *Phys. Rev. B* **44**, 10222 (1991).
- [25] S.J. Hagen, Z.Z. Wang, and N.P. Ong, *Phys. Rev. B* **40**, 9389 (1989).
- [26] Q. Hu and P.L. Richards, *Appl. Phys. Lett.* **55**, 2444 (1989).
- [27] M. Lindgren, M.A. Zorin, V. Trifonov, M. Danerud, D. Winkler, B.S. Karasik, G.N. Gol'tsman, and E.M. Gershenzon, *Appl. Phys. Lett.*, **65**, 3398 (1994).
- [28] N. Perrin and C. Vanneste, *Phys. Rev. B* **28**, 5150 (1983).
- [29] V.A. Trifonov, B.S. Karasik, M.A. Zorin, G.N. Gol'tsman, E.M. Gershenzon, M. Lindgren, M. Danerud, and D. Winkler, *Appl. Phys. Lett.* **68**, 1418 (1996).
- [30] E.M. Gershenzon, G.N. Gol'tsman, A.D. Semenov, and A.V. Sergeev, *Solid State Commun.* **76**, 493 (1990).
- [31] H. Ekström, B.S. Karasik, E. Kollberg, and K.S. Yngvesson, *IEEE Trans. Microwave Theory and Techniques* **43**, 938 (1995).

- [32] B.S. Karasik and A.I. Elantev, *Appl. Phys. Lett.* **68**, 853 (1996); *Proc. 6th Int.Symp. on Space Terahertz Technology*, 21-23 March 1995, Caltech, Pasadena, pp. 229-246.
- [33] J.C. Mather, *Appl. Opt.* **21**, 1125 (1982).

Table Physical parameters of YBCO at 90 K.

---

Electron specific heat		
$c_e, \text{J K}^{-2} \text{cm}^{-3}$	0.025	Ref. 19
Phonon specific heat		
$c_p, \text{J K}^{-2} \text{cm}^{-3}$	0.65	Ref. 20
Phonon thermal conductivity (in a-b plane)		
$\kappa_p, \text{W K}^{-1} \text{cm}^{-1}$	0.1	Ref. 25
Electron thermal conductivity (in a-b plane)		
$\kappa_e, \text{W K}^{-1} \text{cm}^{-1}$	0.01	Ref. 18
Thermal boundary resistance (MgO substrate)		
$R_p, \text{K cm}^2 \text{W}^{-1}$	$5.0 \times 10^{-4}$	Ref. 21, 22

---

Table 2. Parameters of the optimum operating points.

Point #	$T, K$	$P_{LO}, \mu W$	$T_M, K$	$\eta, dB$	$R, \Omega$	$I, \mu A$	$Z(2.5GHz), \Omega$	$Z(0), \Omega$
1	66	II	2200	4.3.1	63	56	104-28j	145
2	77	4.9	5200	-5.1	118	41	162-27j	197

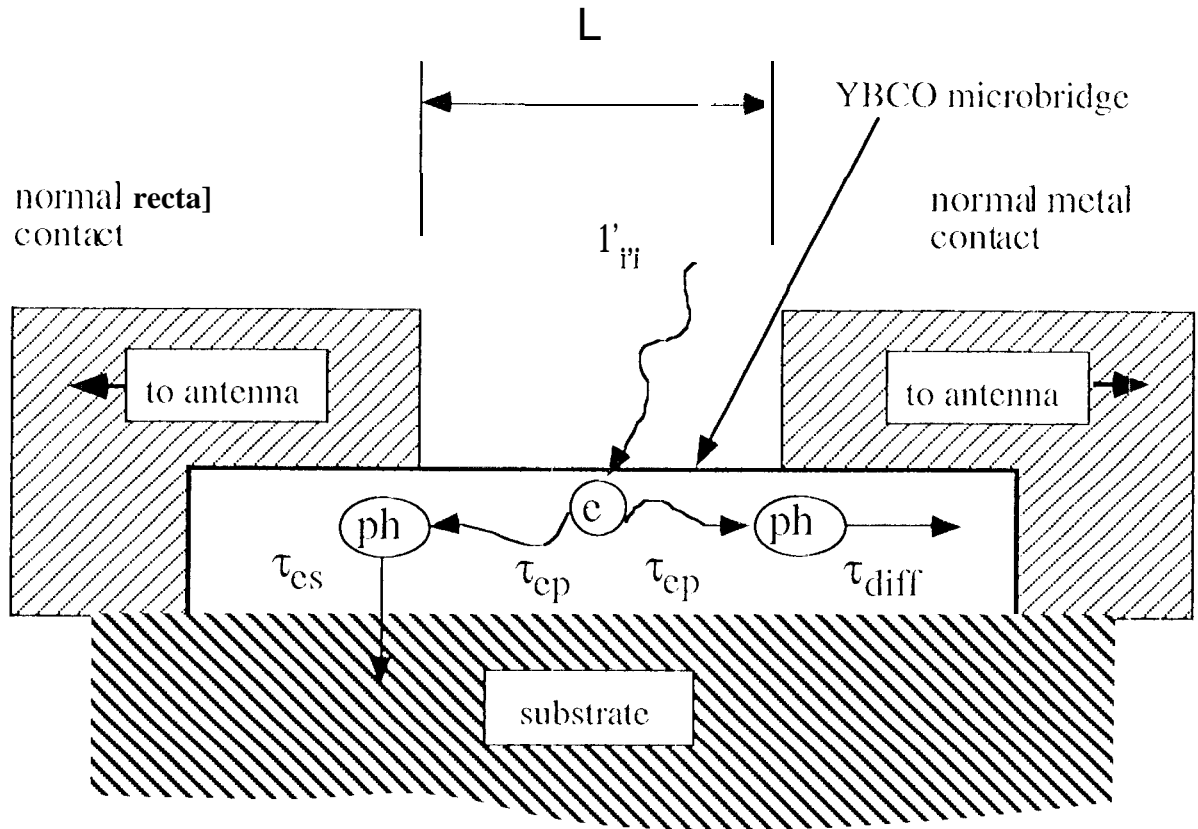


Fig. 1. Flow-diagram of elementary processes in YBCO film: electrons ( $e$ ) absorbing rf power  $I'_{rf}$ , couple to phonons ( $ph$ ) during  $\tau_{ep}$ , then phonons can either diffuse to the contacts or escape to the substrate and diffuse away

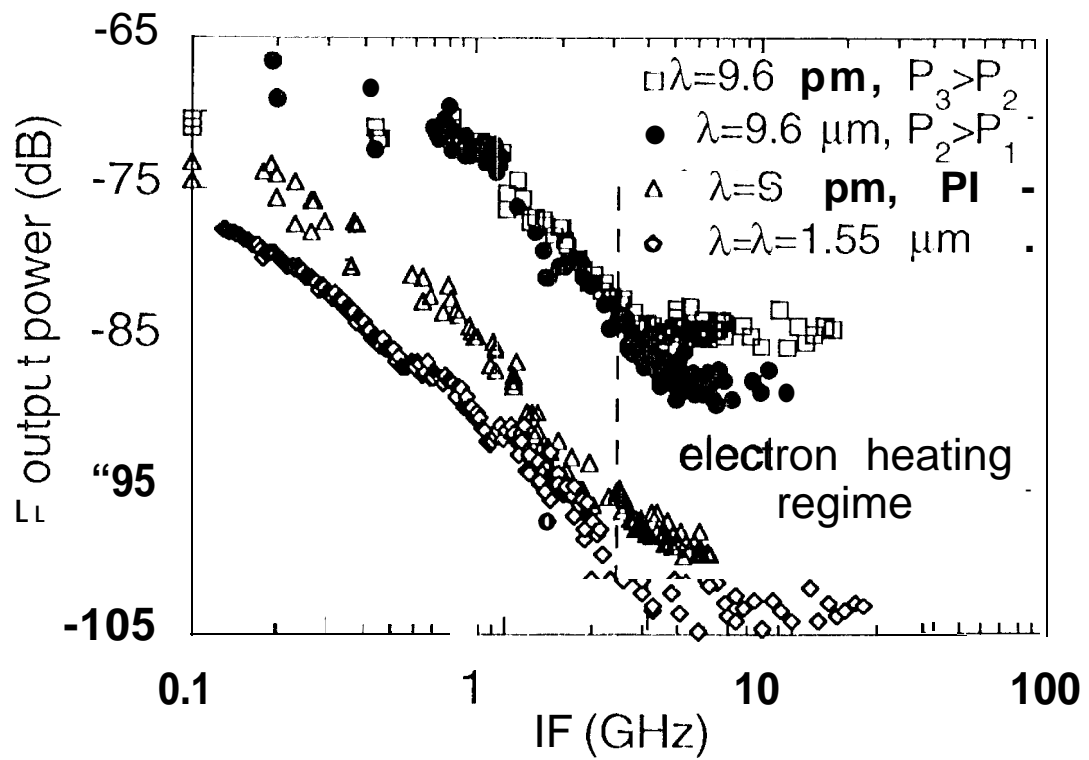
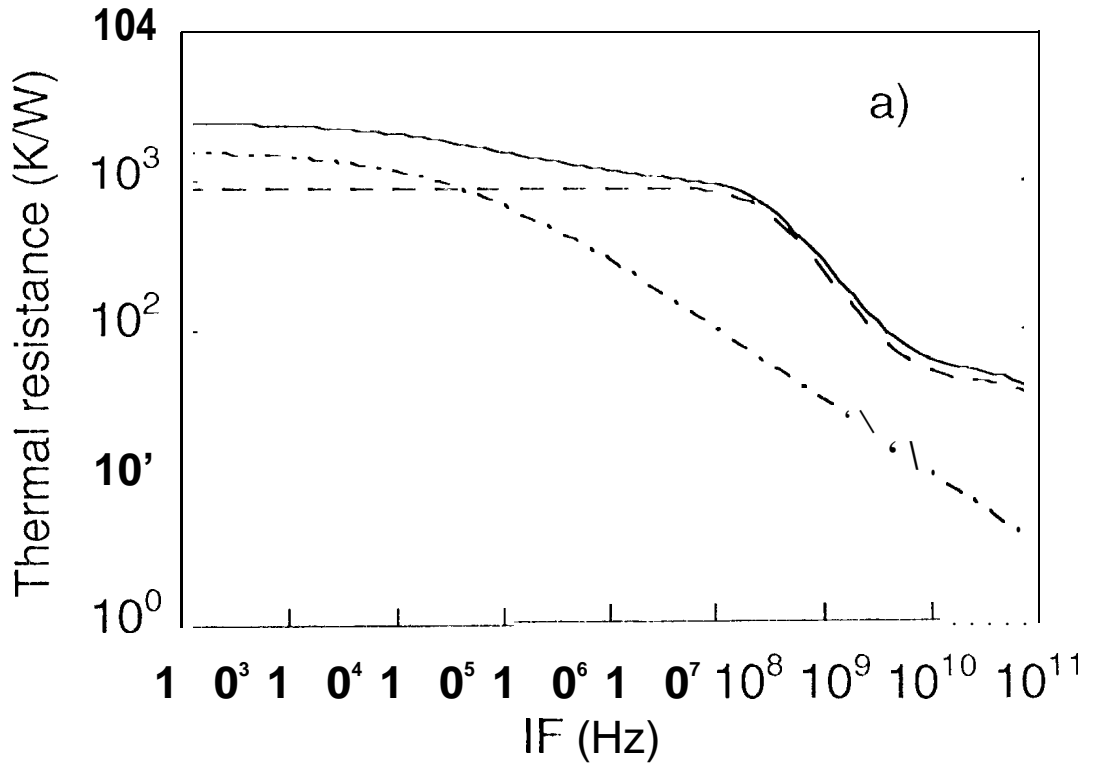
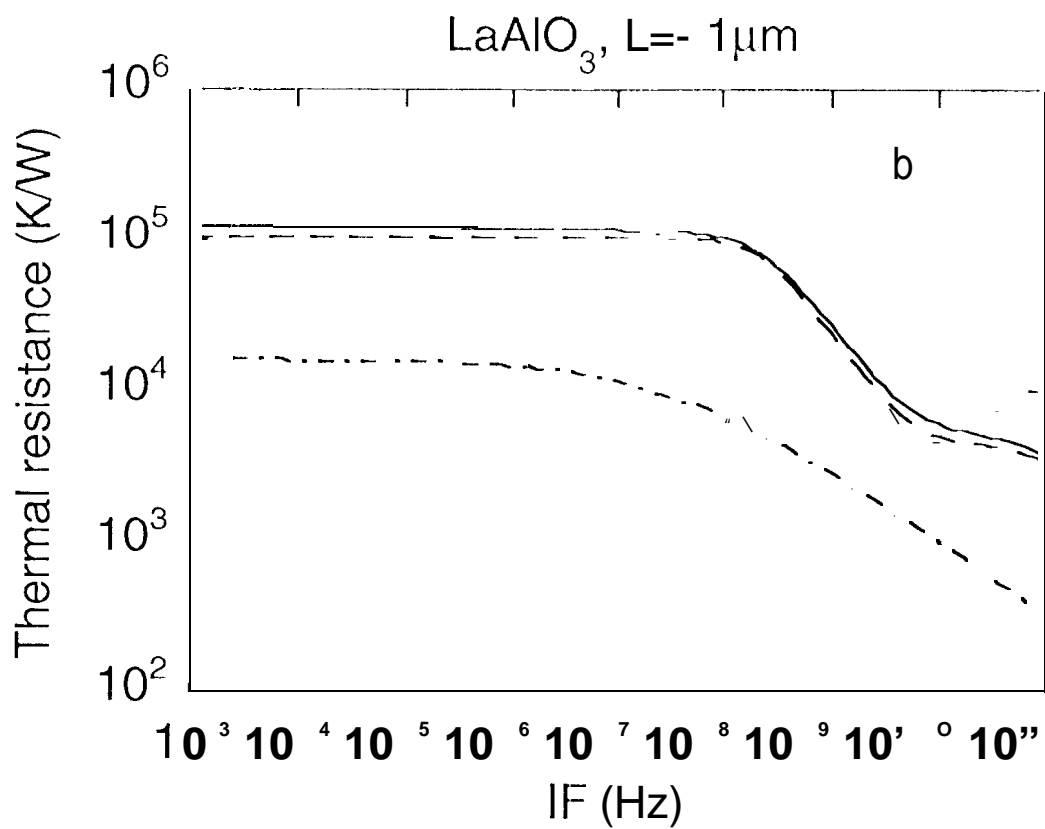
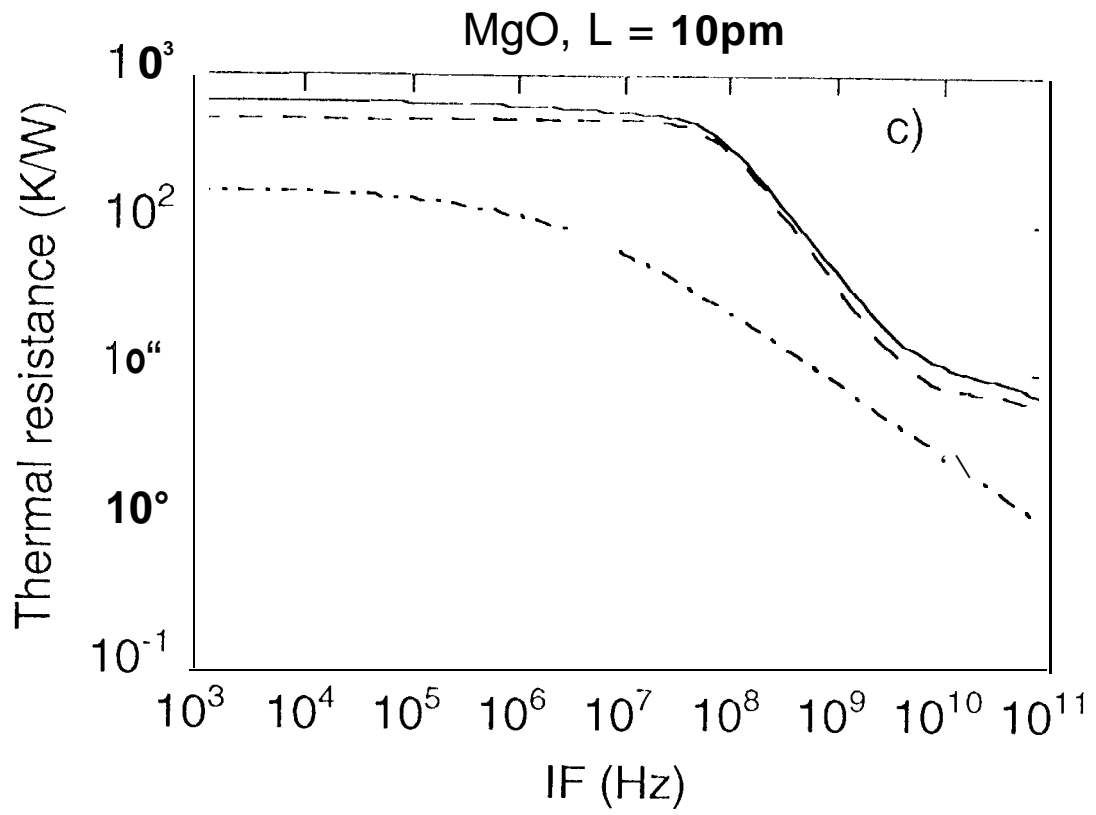


Fig. 2. Data on optical mixing in YBCO films (Ref's. 27,29). The three curves for  $\lambda=9.6 \mu\text{m}$  correspond to different levels of 1.0 power  $P$ .

LaA10<sub>3</sub>, L = 10pm







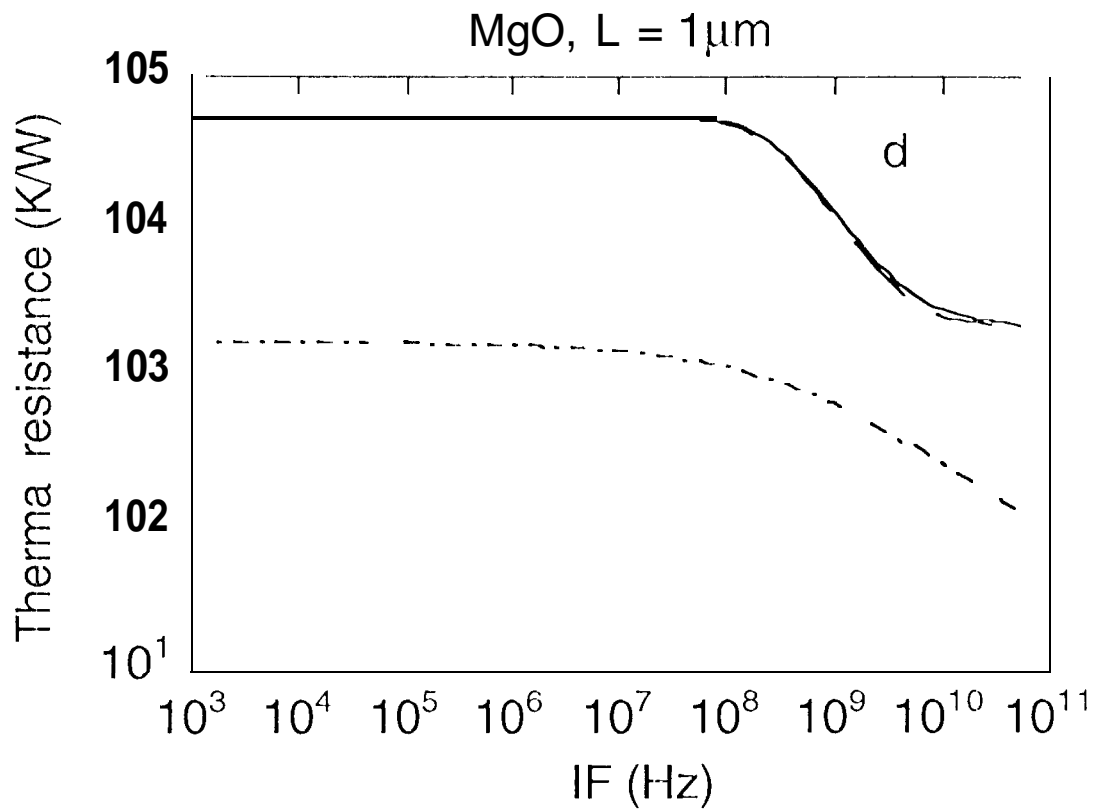


Fig 3. Thermal resistance in a 10 nm thick YBCO film/substrate system. Total resistance,  $R_{top}$  - solid line, between electrons and substrate,  $R_{e-s}$  - dashes, substrate,  $R_s$  - dashed-and-dotted line.

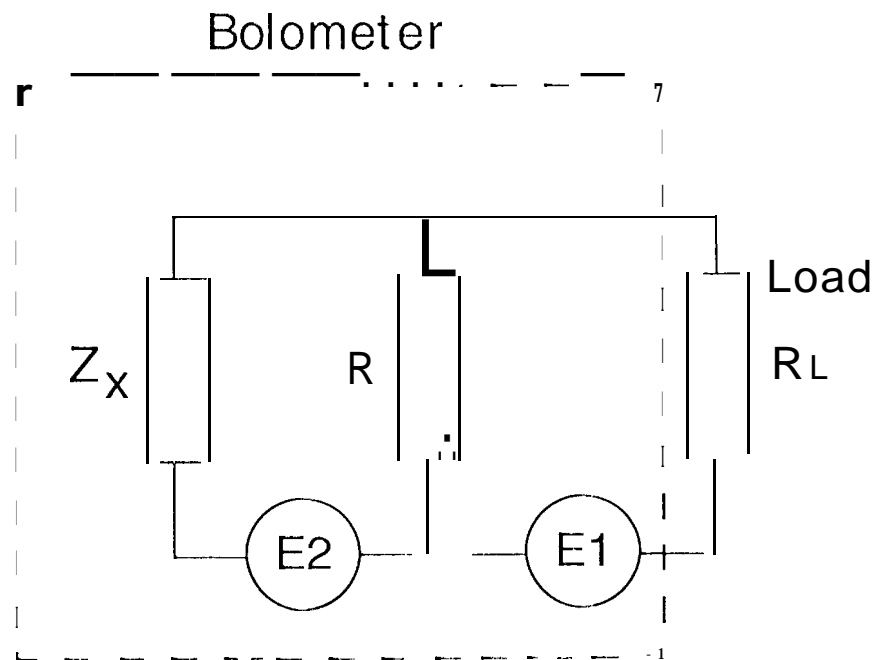
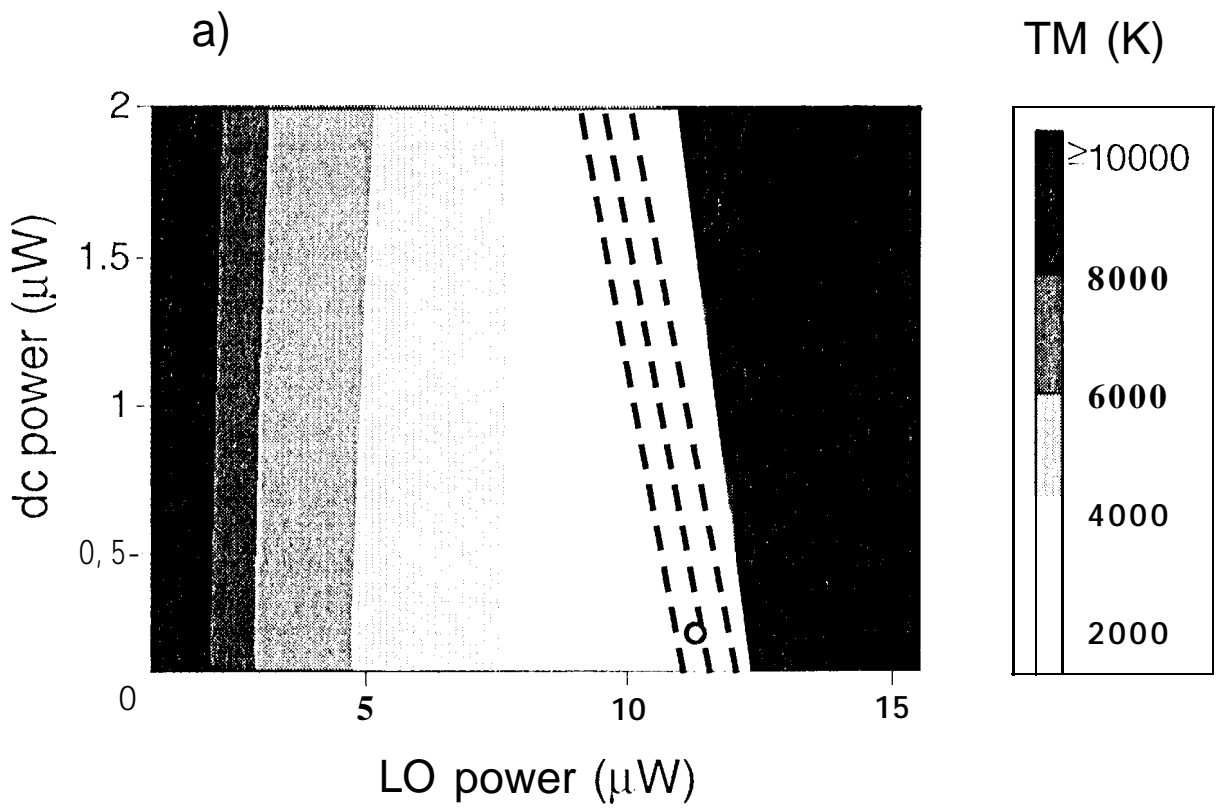


Fig.4. Equivalent circuit for calculations of the Johnson noise temperature in a bolometer.



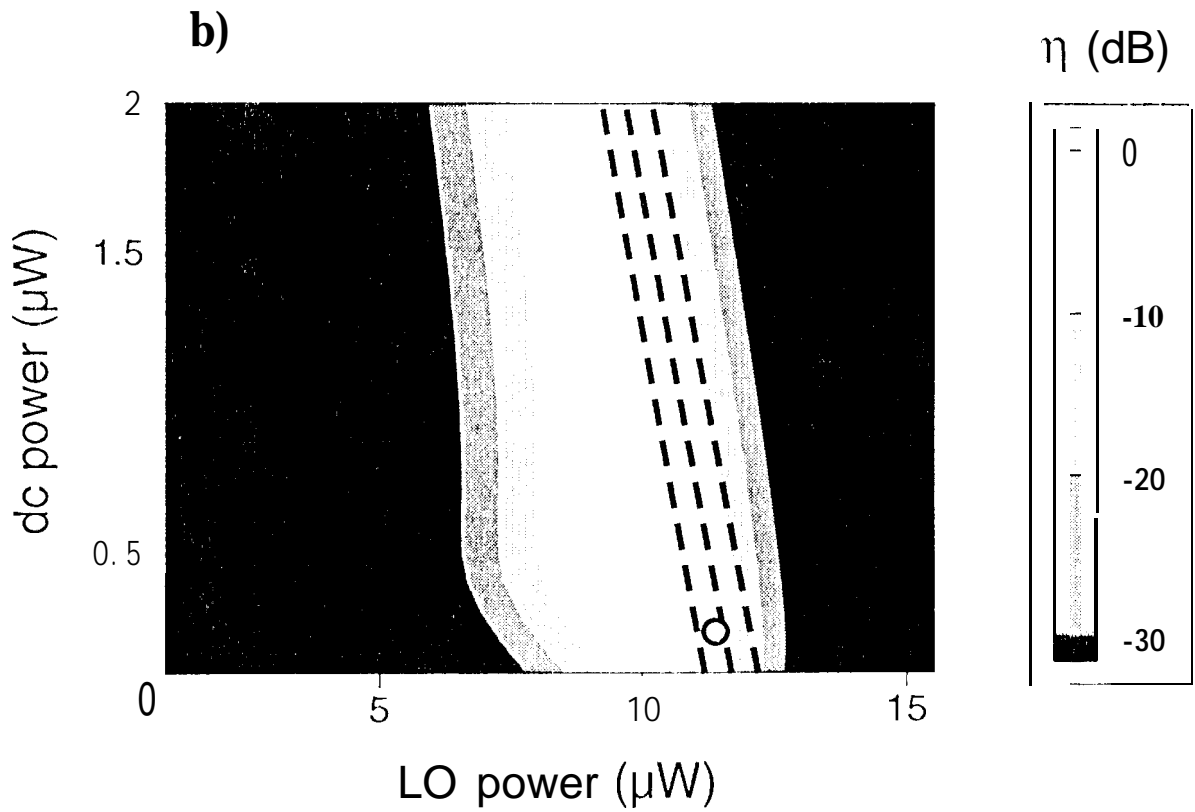


Fig. 5. Mixer noise temperature (a) and mixer conversion efficiency (b) vs LO and dc powers. Three dashed lines represent the equal resistance states (from left to right  $0.25R_n$ ,  $0.5R_n$ , and  $0.75R_n$ ). The position of the optimal operating point (minimum  $T_M$ ) is marked with a circle.

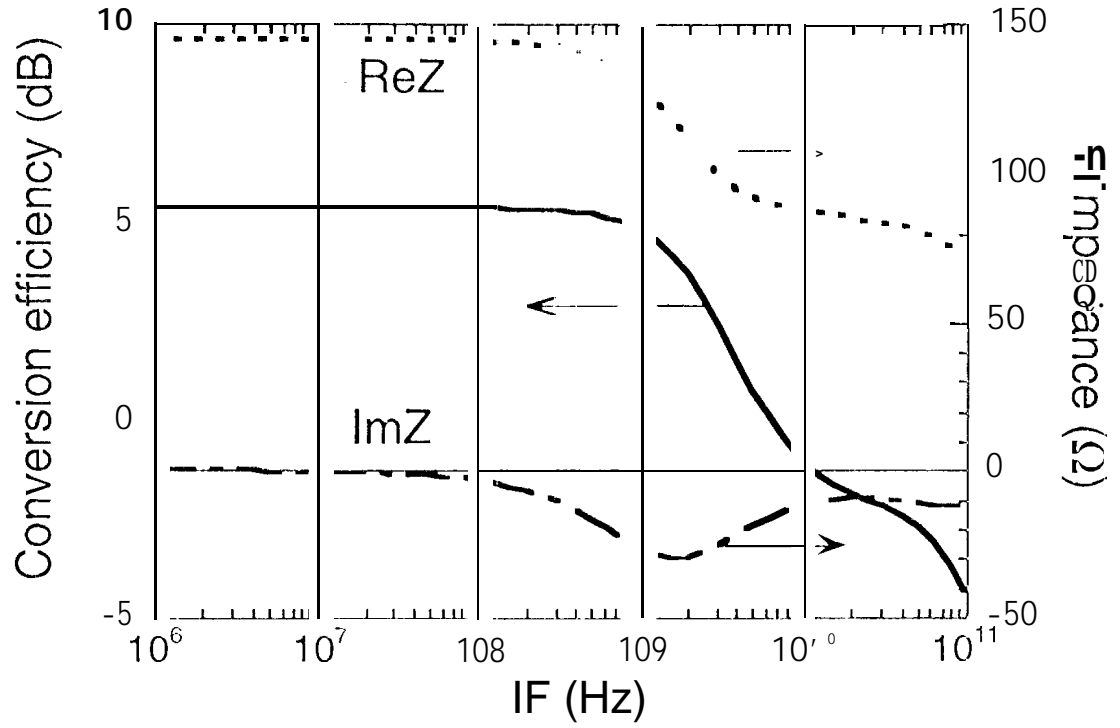


Fig. 6. Conversion efficiency vs IF and the IF impedance at optimal operating point.

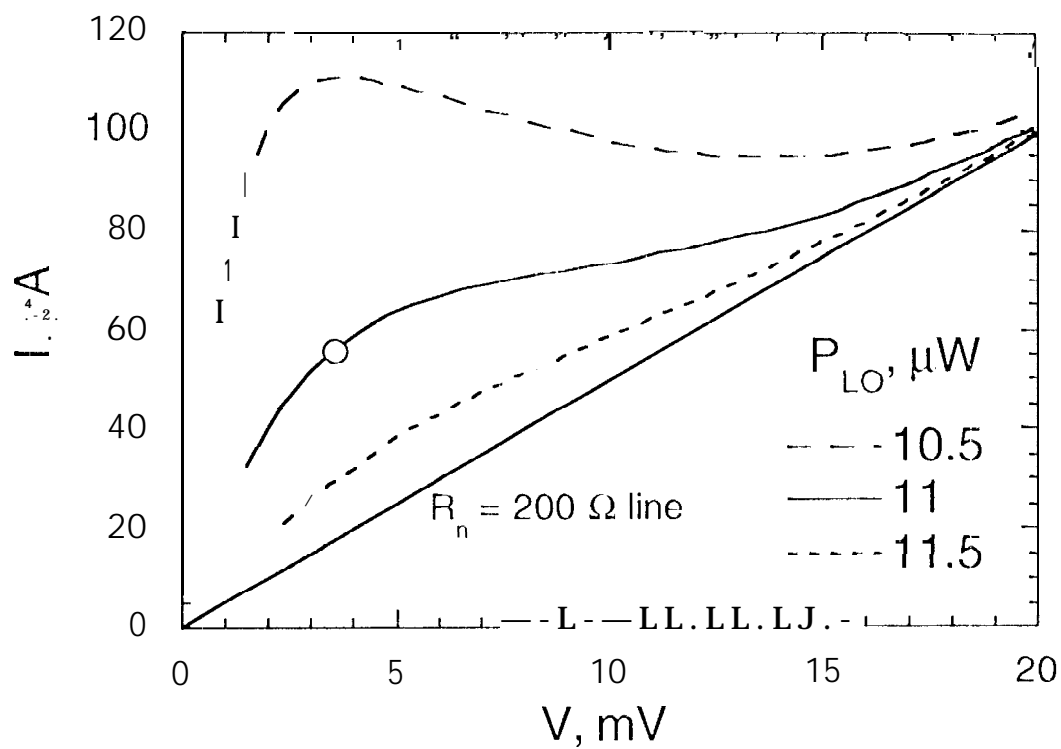


Fig. 7. IV characteristics under different pumping conditions at  $T = 66\text{K}$  ( $L = 0.1 \mu\text{m}$ ,  $d = 10 \text{ nm}$ ). The circle on the optimally pumped curve ( $P_{LO} = 11 \mu\text{W}$ ) represents the position of the bias point.

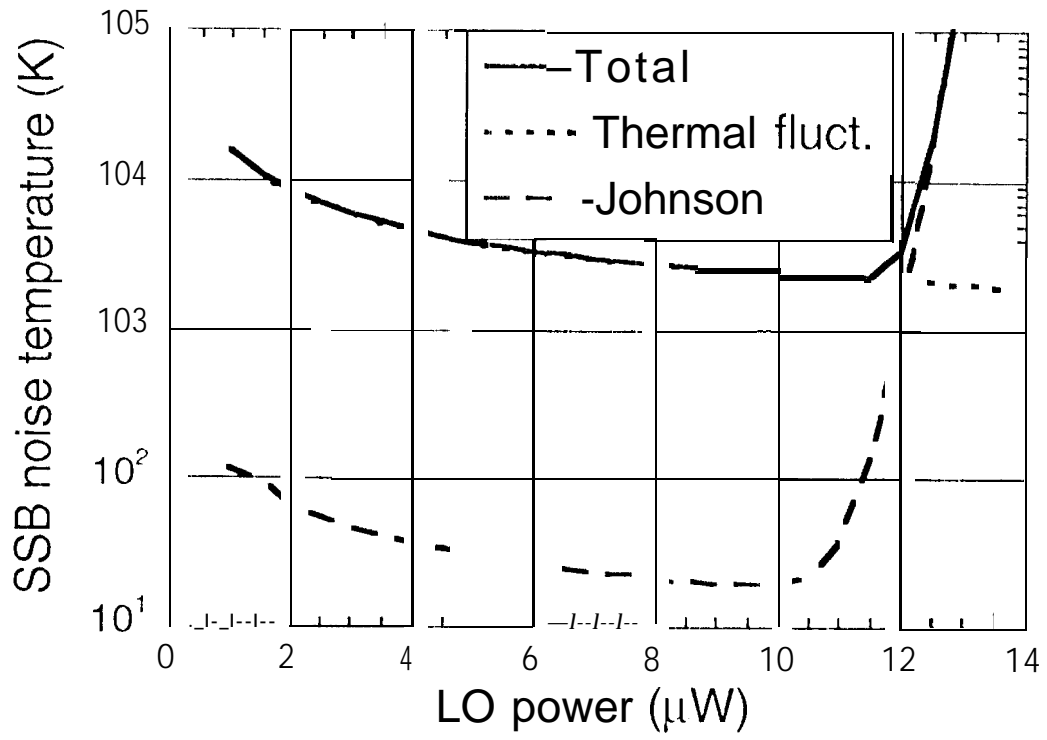


Fig. 8. Noise temperature as a function of the LO power in the vicinity of the optimum point.

$$T = 66 \text{ K}, d = 10 \text{ nm}, L = 0.1 \mu\text{m}$$

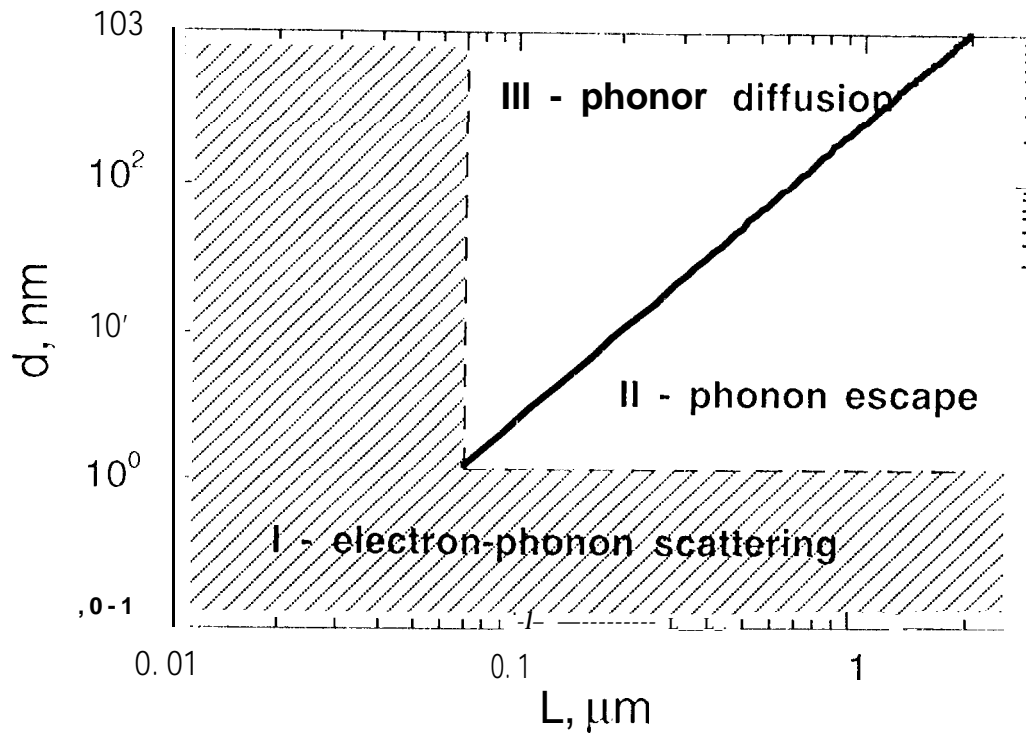


Fig. 9. Dominant mechanisms of heat removal vs HEB device sizes:  $L$  is the bridge length, and  $d$  is the thickness.

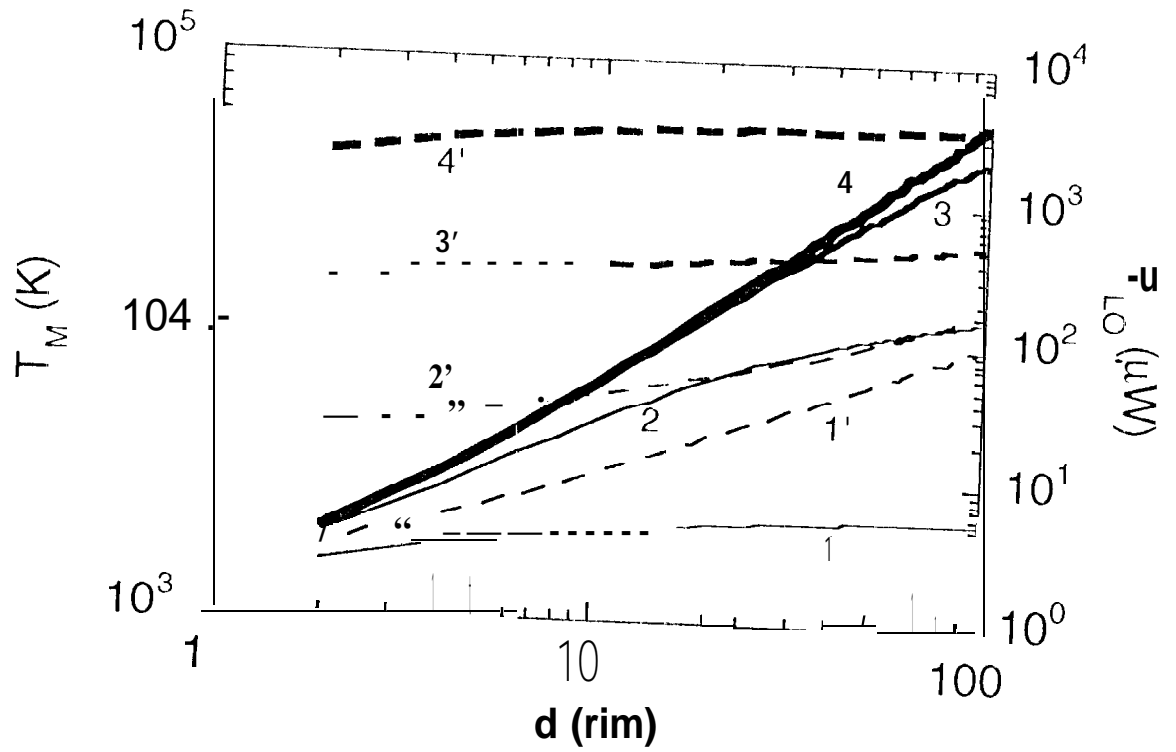


Fig. 10. Size dependence of the mixer noise temperature (solid lines) and optimal I.O. power (dashes).

1 and 1',  $L = 0.1 \mu\text{m}$ ; 2 and 2',  $L = 0.3 \mu\text{m}$ ; 3 and 3',  $L = 1.0 \mu\text{m}$ ; 4 and 4',  $L = 3.0 \mu\text{m}$ .

$T = 66 \text{ K}$ .

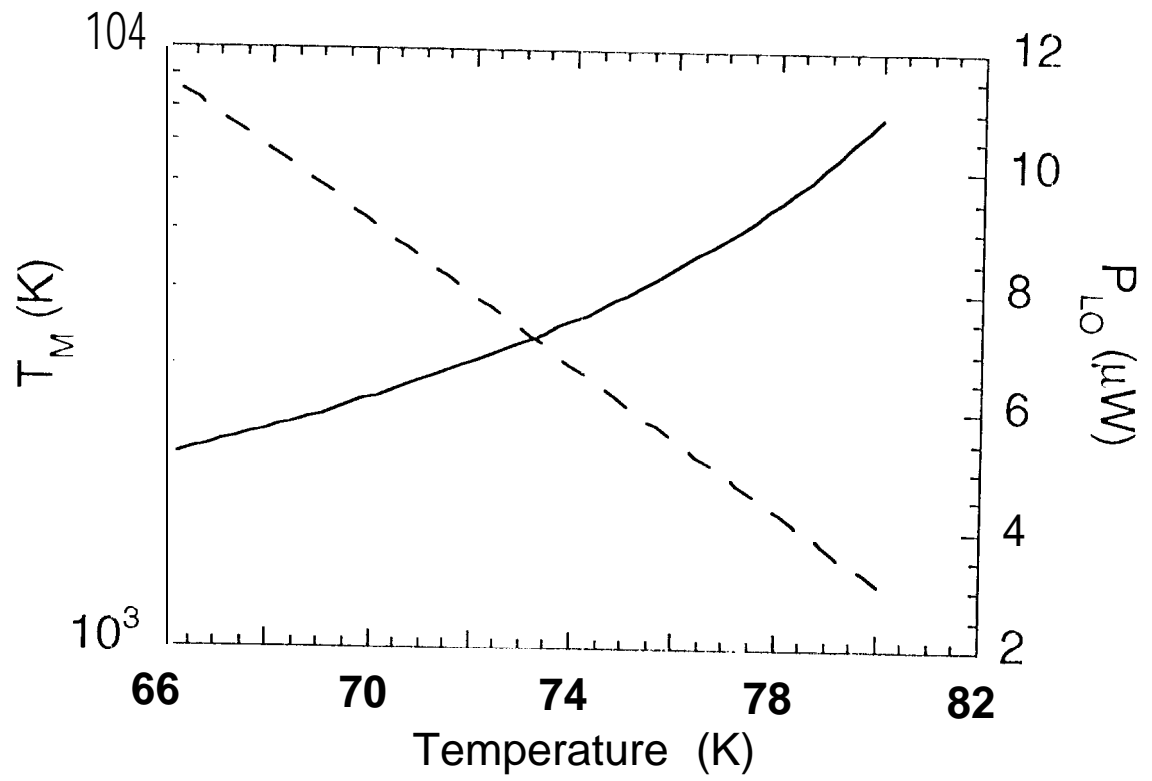


Fig.11. Temperature dependence of the mixer noise temperature and optimal LO power.

$$L = 0.1 \mu\text{m}, d = 10 \text{ nm}.$$